Title
Chorus intensity modulation driven by time-varying field-aligned low-energy plasma

Journal
Journal of Geophysical Research: Space Physics, 120(9)

ISSN
2169-9380

Authors
Nishimura, Y
Bortnik, J
Li, W
et al.

Publication Date
2015-09-01

DOI
10.1002/2015JA021330

Peer reviewed

AGU PUBLICATIONS

JGR

Journal of Geophysical Research: Space Physics

RESEARCH ARTICLE
10.1002/2015JA021330

Special Section:
Pulsating Aurora and Related Magnetospheric Phenomena

Chorus intensity modulation driven by time-varying field-aligned low-energy plasma

Y. Nishimura[1], J. Bortnik[1], W. Li[1], J. Liang[2], R. M. Thorne[1], V. Angelopoulos[3], O. Le Contel[4], U. Auster[5], and J. W. Bonnell[6]

[1]Department of Atmospheric and Oceanic Sciences, University of California, Los Angeles, California, USA, [2]Department of Physics and Astronomy, University of Calgary, Calgary, Alberta, Canada, [3]Department of Earth, Planetary and Space Sciences, University of California, Los Angeles, California, USA, [4]Laboratoire de Physique des Plasmas, CNRS/Ecole Polytechnique/UPMC/Paris-Sud, Palaiseau, France, [5]Institut für Geophysik und extraterrestrische Physik, Technischen Universität Braunschweig, Braunschweig, Germany, [6]Space Sciences Laboratory, University of California, Berkeley, California, USA

Key Points:
- Chorus modulation is found to correlate with field-aligned low-energy plasma
- The density modulation contributes to chorus wave growth
- Ionospheric source is suggested for low-energy plasma and chorus modulation

Correspondence to:
Y. Nishimura,
toshi@atmos.ucla.edu

Citation:
Nishimura, Y., J. Bortnik, W. Li, J. Liang, R. M. Thorne, V. Angelopoulos, O. Le Contel, U. Auster, and J. W. Bonnell (2015), Chorus intensity modulation driven by time-varying field-aligned low-energy plasma, *J. Geophys. Res. Space Physics*, *120*, 7433–7446, doi:10.1002/2015JA021330.

Received 13 APR 2015
Accepted 19 AUG 2015
Accepted article online 22 AUG 2015
Published online 18 SEP 2015

Abstract Recent studies have shown that chorus waves are responsible for scattering and precipitating the energetic electrons that drive the pulsating aurora. While some of the chorus intensity modulation events are correlated with <~100 eV electron density modulation, most of the chorus intensity modulation events in the postmidnight sector occur without apparent density changes. Although it is generally difficult to measure evolution of low-energy (<~20 eV) electron fluxes due to constraints imposed by the spacecraft potential and electrostatic analyzer (ESA) energy range limit, we identified using Time History of Events and Macroscale Interactions during Substorms (THEMIS) satellite data that low-energy ions of ~100 eV show density modulation that is correlated with chorus intensity modulation. Those low-energy ions and electrons are field-aligned with major peaks in 0° (for northern hemisphere winter event) and 180° (for northern hemisphere summer event) pitch angle, indicating that outflowing plasma from the sunlit hemisphere is the source of the low-energy plasma density modulation near the equator. Plasma sheet plasma density, and ambient electric and magnetic fields do not show modulations that are correlated with the chorus intensity modulation. Assuming charge neutrality, the low-energy ions can be used to represent cold plasma density in wave growth rate calculations, and the enhancements of the low-energy plasma density are found to contribute most effectively to chorus linear growth rates. These results suggest that chorus intensity modulation is driven by a feedback process where outflowing plasma due to energetic electron precipitation increases the equatorial density that drives further electron precipitation.

1. Introduction

Chorus waves are known to effectively scatter plasma sheet electrons (~1–10 keV) that subsequently precipitate into the atmosphere and generate diffuse aurora [*Thorne et al.*, 2010; *Ni et al.*, 2011]. Chorus waves and precipitating energetic electrons often show fast (a fraction of a second) and slow (a few seconds to tens of seconds) intensity modulations [*Li et al.*, 2013a; *Tsurutani et al.*, 2013, and references therein]. The fast modulation corresponds to the recurrence periods of individual rising or falling tone elements in chorus waves, and nonlinear wave-particle interaction has been considered as the cause of the modulation [e.g., *Omura et al.*, 2008]. The slow modulation with periods between a few and a few tens of seconds consists of a group of chorus elements switching on and off quasiperiodically. Although several mechanisms have been proposed to explain the cause of this modulation, it has been a long-standing question for understanding the generation mechanism of chorus waves.

Chorus waves have been considered as one of the candidate wave modes that drive pulsating aurora, based on correlations between ELF/VLF intensity and auroral luminosity [*Tsuruda et al.*, 1981; *Johnstone*, 1983; *Tagirov et al.*, 1999]. Although it has been rare to observe equatorial and auroral regions simultaneously and to precisely treat magnetic field line modeling, recent studies by *Nishimura et al.* [2010, 2011] determined magnetic field mapping and identified uniquely that lower band chorus is responsible for driving pulsating aurora. Thus, the study of chorus intensity modulation has a direct impact on understanding the driver of auroral pulsation.

Li et al. [2011] presented a type of chorus intensity modulation that occurs preferentially in the dawn to noon sector. Chorus intensity of those events was found to correlate strongly with <~100 eV plasma density, while

plasma sheet electrons do not show notable changes. Electron densities of <~100 eV electrons during chorus intensifications (chorus "on" times) are several times larger than during chorus "off" times. This is consistent with linear growth rate calculations that enhanced cold plasma density is favorable for larger linear growth rates, when the ratio of the cold and hot plasma densities is below a certain level [*Cuperman and Landau*, 1974; *Wu et al*., 2013]. Nonlinear models (relaxation oscillator [*Davidson and Chiu*, 1987] and flowing cyclotron maser [*Demekhov and Trakhtengerts*, 1994]) suggest that periodic chorus intensity modulation can occur in enhanced density ducts and thus chorus intensity modulations and related pulsating aurora in the high-density flux tubes could be driven spontaneously.

In contrast, a large number of chorus intensity modulation events particularly in the postmidnight sector do not show notable changes in <~100 eV electrons [*Li et al*., 2011]. Those events instead show total density reductions based on spacecraft potential measurements. However, such density reductions are not seen in particle observations and may be an artificial effect because of photoelectron escaping due to intense chorus electric fields [*Malaspina et al*., 2014]. Then the question arises as to what drives chorus intensity modulation and, if it is related to a certain particle population, whether we can directly identify such a population in particle data.

In the present study, we select four of such events from Time History of Events and Macroscale Interactions during Substorms (THEMIS) where <~100 eV omnidirectional electron fluxes do not show apparent enhancements in correlation with chorus intensity modulation. Since it is generally difficult to observe evolution of <~20 eV electron fluxes due to constraints imposed by the spacecraft potential and electrostatic analyzer (ESA) energy range limit, we also examine ion data for identifying possible modulation of cold plasma by assuming charge neutrality. We identify that field-aligned low-energy ions of ~100 eV show small-density modulation that is correlated with chorus intensifications. Those ions are observed to travel preferentially from the summer to winter hemisphere, indicating that ion outflows from the sunlit ionosphere modulate equatorial plasma density and the growth rate of chorus waves.

2. Method and Data Set

The search coil magnetometer (SCM) [Le *Contel et al*., 2008] on board the THEMIS satellites [*Angelopoulos*, 2008] provides magnetic field spectra. The electron cyclotron frequency (f_c) is obtained from the magnetic field instrument (fluxgate magnetometer (FGM)) [*Auster et al*., 2008] and is used to identify lower band chorus waves (0.05–0.5 f_c). Since all the events shown in this paper are obtained within 5° magnetic latitude from the equator, the use of local f_c gives a reasonable estimate of equatorial f_c and does not introduce significant errors in identification of lower band chorus, and it can be considered that the satellites are located near the chorus generation region. Electron and ion distributions are provided by the electrostatic analyzer (ESA) [*McFadden et al*., 2008] and solid state telescope (SST). The pitch angles are calculated with an aid of the FGM data. The Electric Field Instrument [*Bonnell et al*., 2008] measures the electric field and spacecraft potential. We use particle burst mode data, where wave spectrograms (provided by the digital field box [*Cully et al*., 2008]) and particles are observed in 1 and 3 s cadences.

Following the approach by *Li et al*. [2011], we split the chorus linear growth rate given by *Kennel and Petschek* [1966] into two parts:

$$\gamma/|\Omega_e| = \pi R(V_R)\cdot[A(V_R) - A_c] \tag{1}$$

where γ, Ω_e, V_R, $A(V_R)$, and A_c are the linear wave growth rate, electron cyclotron angular frequency, resonant velocity, anisotropy of resonant electrons, and critical anisotropy, respectively. R is defined as

$$R(V_R) = \left(1 - \frac{\omega}{|\Omega_e|}\right)^2 2\pi \frac{|\Omega_e| - \omega}{k} \int_0^\infty v_\perp d^\perp v_\perp f^\perp\left(v_\perp, {}^\perp v_{||} = V_R\right). \tag{2}$$

Note that k and V_R also depend on the total density through the dispersion relation. Thus, the wave growth rate expressed through R increases (decreases) with density when cold plasma population is small (large) for a given constant anisotropy [*Wu et al*., 2013]. Measured ESA and SST electron fluxes are used to obtain the distribution function of plasma sheet plasma. Since only part of the cold electrons can be measured in ESA, we used ESA ion density below 100 eV for event 1, and below 300 eV for event 2 to represent the cold plasma density, assuming charge neutrality. *Li et al*. [2011] showed that, while the plasma sheet electrons

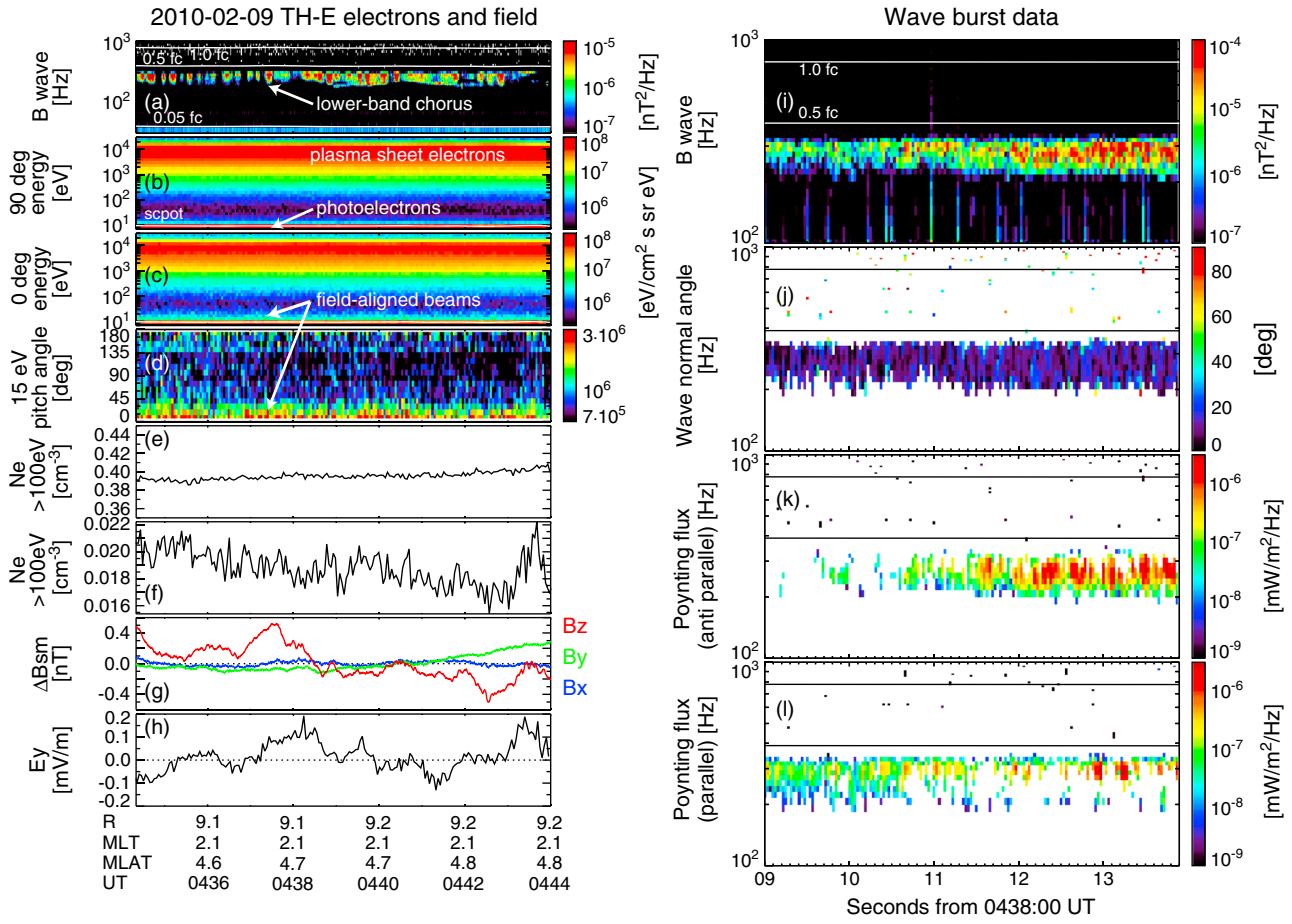

Figure 1. TH-E observations of (a) magnetic field spectra, energy distribution of (b) 90 and (c) 0° pitch angle electron fluxes, (d) pitch angle distribution of 15 eV electrons, density moments of (e) >100 and (f) <100 eV electrons, (g) ambient magnetic field deviation from the mean, and (h) dawn-dusk electric field on 9 February 2010. The white lines in Figure 1a are 1.0, 0.5, and 0.05 local electron gyrofrequency. The spacecraft potential (~9.5 V) is shown in white in Figures 1b and 1c. (i–l) Wave burst data during one of the chorus bursts. From top to bottom, panels shown are wave magnetic field intensity, wave normal angle, and Poynting flux antiparallel and parallel to ambient magnetic field.

do not show notable changes, the *A* parameter shows variations uncorrelated with chorus intensity modulation due probably to noise in the observations. Since such variations obscure density effects on the growth rate, we use the *R* parameter as a proxy of the linear growth rate.

3. Results

3.1. Event 1: 9 February 2010

Figure 1 shows wave spectra, electron energy fluxes, and ambient electric and magnetic fields measured by TH-E during the 9 February 2010 event. The satellite was located near the equator in the postmidnight sector. Intensity modulation of lower band chorus waves in an ~10–20 s periodicity is evident in Figure 1a. Wave burst data are available for one of the chorus bursts soon after 04:38:00 UT. The wave normal angle is <~10° (Figure 1j), indicating that the chorus waves propagate essentially along the ambient magnetic field. A notable feature is large Poynting fluxes seen in both parallel and antiparallel directions relative to the magnetic field (Figures 1k and 1l). Since chorus Poynting fluxes are unidirectional, and point away from a source region [e.g., *Santolík et al.*, 2004], the bidirectional Poynting fluxes indicate that the satellite was located near the chorus generation region (slightly to the north of its center). See *Li et al.* [2013b] for details of wave normal angle and Poynting flux calculations.

Plasma sheet electron fluxes (~>100 eV in Figures 1b and 1c) and their density moment (Figure 1e) are essentially steady without any notable change that is correlated with chorus intensity modulation. On the other hand, by comparing Figures 1b and 1c below 20 eV, one can see the existence of low-energy electrons in

the field-aligned direction. The pitch angle distribution at 15 eV (Figure 1d) shows that those populations are unidirectional, traveling toward the northern hemisphere. The field-aligned energy flux near 0° pitch angle shows modulations with a similar period range to the chorus intensity modulation. The field-aligned flux modulation is much larger than that seen near 90° pitch angle, and thus, this modulation is not a result of instrumental noise. The density moment below 100 eV (Figure 1f) shows modulation with an ~10% amplitude relative to the average of this period, while the fluctuations in the hot plasma density in Figure 1e are just at a level of ~1%. Although the low-energy plasma density (<100 eV) measurable by ESA is much smaller than the hot plasma density (>100 eV), modulation in the low-energy plasma density can influence the ratio of the cold and hot densities that controls the wave growth rate. However, the low-energy plasma density shown here is likely underestimated because it is difficult to calculate the moment accurately in the presence of photoelectrons, which can be seen below 10 eV.

The ambient magnetic and electric fields do not show oscillations that are correlated with chorus intensity modulation. The correlation coefficient of wave intensity and B_z (E_y) is −0.14 (−0.07). This is consistent with *Oguti et al*. [1986] and *Li et al*. [2011] and indicates that the chorus intensity modulation is not due to ULF waves.

To overcome some of the difficulties involved in calculating the cold electron density, we investigated ion distributions during this time period (Figure 2). While the energy distribution at 90° pitch angle only shows plasma sheet ions of ~10 keV (Figure 2b), the 0° distribution shows a distinct low-energy ion beam below 100 eV (Figure 2c). This low-energy population is confined near 0° pitch angle, and the 0° fluxes are larger than the 180° fluxes (Figures 2d and 2e). The ratio between 0 and 180° fluxes is 1.2. This pitch angle distribution is similar to that of the low-energy electrons shown in Figure 1d, suggesting that those ions and electrons have the same source region. Such field-aligned ions have been related to ion outflows from the ionosphere [*Horwitz et al*., 1982; *Chappell et al*., 2008]. Unlike the low-energy electrons, those ions are covered fully within the ESA energy range well above the spacecraft potential, and thus, the density moment can be calculated more accurately. The ion density moment below 100 eV (Figure 2f) is a factor of 4 larger than the low-energy electron density (Figure 1f), and the density modulation can be seen more clearly. The density modulation is likely real, because the background noise level seen around the 90° pitch angle is fairly steady and is much smaller than the field-aligned fluxes (Figure 2e). The higher-density moment for ions demonstrates that the low-energy plasma density of this event is obtained more accurately from ions than from electrons.

Assuming charge neutrality between the low-energy electrons and ions, the low-energy ion density can be used to represent the cold plasma density. A comparison of Figures 1e and 2g shows that plasma sheet electron and ion densities are around 0.39–0.4 cm^{-3} and that any notable difference between those densities (~0.01–0.02 cm^{-3}) is much smaller than the low-energy ion density (~0.08–0.1 cm^{-3}). This means that plasma sheet ions and electrons have essentially the same density and suggests that the measured low-energy ions are in charge neutrality with hidden low-energy electrons. The low-energy ion density is added to the distribution function in equation (2) as cold plasma density for calculating the R parameter. The assumption of charge neutrality in general applies to the entire plasma distribution, but by considering that low-energy electrons and ions are field-aligned while the hot population is peaked at 90°, the cold ions should maintain charge neutrality with cold electrons and the same for the hot component to maintain charge neutrality everywhere along the entire extent of a flux tube on comparable time scales. Here the ESA instrument does not resolve ion species, and all ions are treated as H^+. This assumption seems reasonable based on the statistics by *Chappell et al*. [2008], who showed that low-energy ions in the postmidnight sector outside the geosynchronous orbit are mainly H^+. Figure 3 shows that the most oscillations in the low-energy ion density are correlated with the chorus intensity modulation. Although the correlation is not perfectly one-to-one, many of the chorus spikes (marked by red arrows in Figure 3b) occur simultaneously with the density enhancements (blue arrows). It is appropriate to consider simultaneous correlation because the satellite is suggested to be within the source region based on the bidirectional Poynting flux (Figures 1k and 1l). It should be noted, however, that timing of the density enhancements has a 3 s uncertainty due to the limited time resolution of ESA. Also, not all chorus bursts are necessarily located close to the satellite. If the source region of a chorus burst is located slightly away from the satellite, the unknown separation introduces a finite time lag due to particle motion (wave propagation is almost instantaneous within the measurement resolution). This may explain slight time delays of the peaks seen for example at 04:39:00 UT.

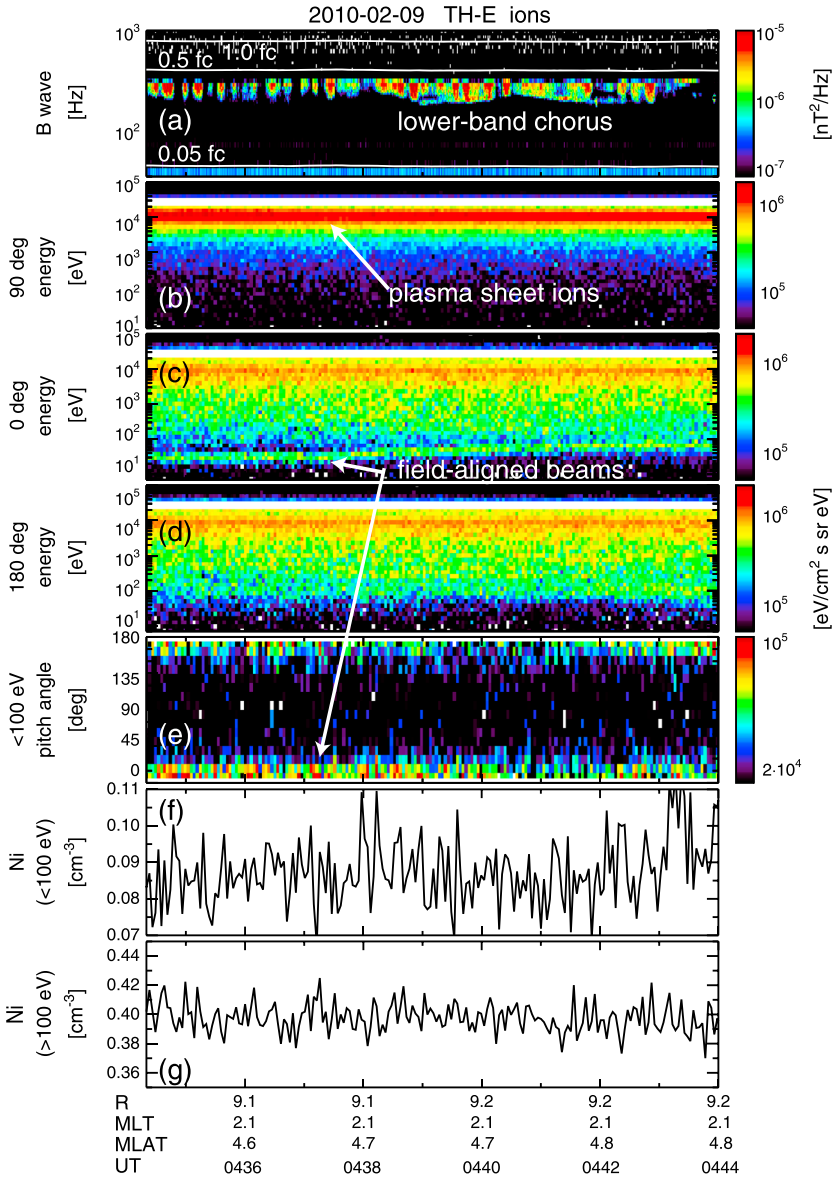

Figure 2. Ion observations during the Figure 1 event. (a) Wave magnetic field spectra, energy distribution of (b) 90 and (c) 0° pitch angle ions, (d) pitch angle distribution of <100 eV ions (maximum energy flux at each pitch angle), (f) density moment of <100 eV ions, and (g) density moment of >100 eV ions.

The *R* parameter using this density (Figure 3c) essentially has the same peaks as the low-energy ion density, indicating that the density modulation can contribute to wave growth. The plasma sheet electron density is almost constant (Figure 3d), and the ambient electric and magnetic fields do not show variations in the period of chorus intensity modulation as in Figure 1. These results suggest that the modulation of the low-energy plasma density may control the chorus growth rate modulation.

Here although the modulations in wave amplitude and plasma density occur with the same periodicity overall, there seems to be no quantitative relation at first between the wave intensity and the plasma density. We should note the limitations of the present observations. Since low-energy ions are field-aligned, only a few solid angle bins of the ESA instrument can detect the field-aligned population. This may cause some uncertainties in the density moment because a change in actual distribution function may be underestimated if the peak of the distribution function falls between two detectors or energy ranges. Also, the wave source region does not necessarily stay at a constant position but may move around along a magnetic field line. Although

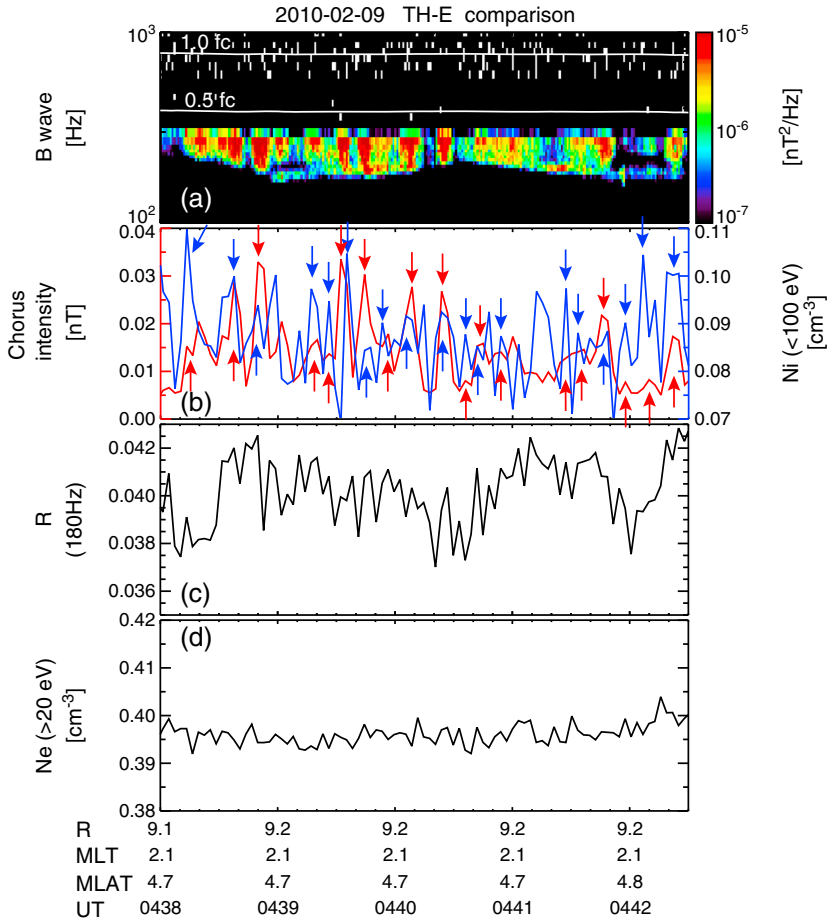

Figure 3. Wave-density comparison of the Figure 1 event. (a) Magnetic field spectra, (b) frequency-integrated lower band chorus intensity (red) and <100 eV ion density moment (blue), (c) *R* parameter calculated for the wave frequency of 180 Hz, and (d) >20 eV electron density moment. The arrows in Figure 3b highlight wave and density pulses that occur simultaneously with each other. The wave intensity data in Figure 3b are decimated to the ESA cadence.

the Poynting flux calculation suggests that the satellites in the present events are close to the source region, a variable source location in pulse-by-pulse basis may introduce variable contributions of wave growth between the source region and satellites.

3.2. Event 2: 12 May 2013

If the low-energy electrons and ions and their pitch angle preference are indeed real as we assume, their directions are expected to show a seasonal variation, dependent on which hemisphere (i.e., auroral ionosphere) is sunlight during the event. This section shows an event observed during northern hemisphere summer to examine if the direction of the field-aligned low-energy plasma changes from the event discussed in section 3.1, which was observed in northern hemisphere winter. This event was also measured in the postmidnight sector and closer to the magnetic equator. The wave instrument detected lower band chorus throughout this time interval (Figure 4a). Wave burst data collected 14 min after this time interval showed wave normal angles of <~10° and Poynting fluxes that propagate both parallel and antiparallel to the ambient magnetic field direction. Similarly to the section 3.1 event, the satellite is suggested to be near the chorus source region, although the satellite is not near the center of the source region due to the much weaker Poynting flux antiparallel to the magnetic field.

The intensity of the chorus waves in the first half of this period changes more slowly (~1 min) than in the second half of the period (~10 s). The slower chorus intensity variations are correlated with the flux of a few tens of eV electrons (Figures 4b). Those electrons are dominantly seen in the 90° pitch angle and

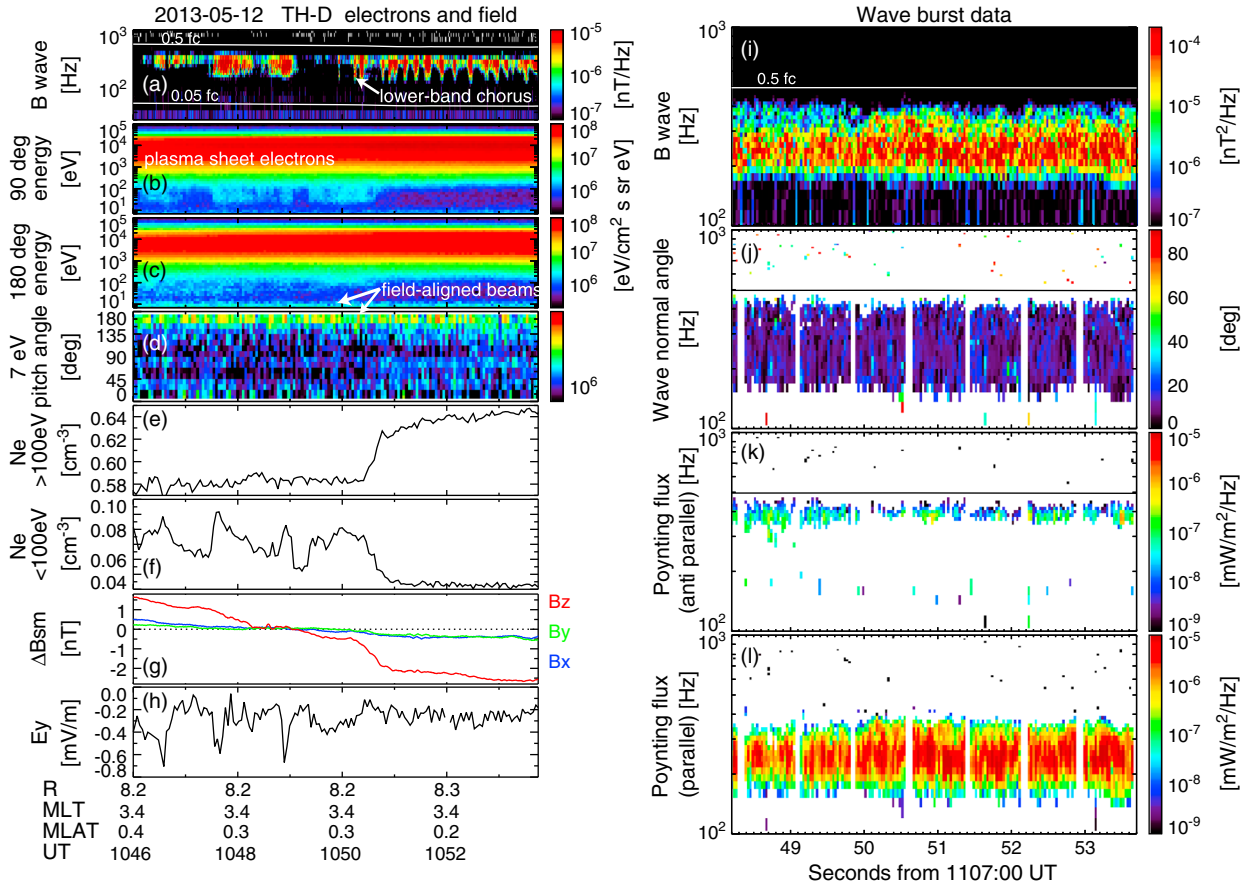

Figure 4. Same as Figure 1 but for 12 May 2013 observed by TH-D. The spacecraft potential is below the ESA energy range (5.5 V).

have large density variations (Figure 4f). This correlation between the chorus intensity and low-energy electron flux in the ESA energy range is consistent with the density enhancement cases studied by *Li et al*. [2011].

The rapid chorus intensity modulation occurs after a few tens of eV electrons disappear. Although the plasma sheet electron density increases abruptly at 10:50:30 UT, the density changes only gradually without large modulation (Figure 4e). The ambient magnetic and electric fields (Figures 4g and 4h) also do not show modulation correlated with chorus intensity modulation. The lack of magnetic field dipolarization suggests that the change at 10:50:30 UT is not due to a fresh injection but to a spatial structure slowly drifting relative to the satellite. The energy distribution of 180° pitch angle electrons shows enhanced fluxes below ~20 eV (Figure 4c). Those electrons are field-aligned in a similar way to the Figure 1 event except for the dominance of the 180° pitch angle electrons. However, this population is seen near the bottom edge of the ESA energy range, and thus, only part of the distribution is covered by the instrument. The ambient magnetic and electric fields do not show variations that are correlated with chorus intensity modulation.

The ion energy spectra in Figures 5c and 5d show distinct low-energy ions below 300 eV in the field-aligned directions. Those ions are not seen in the perpendicular direction, and the 180° pitch angle fluxes are about 30% larger than the 0° fluxes. The opposite directions of low-energy plasma motion in this and the section 3.1 cases indicate that the ionosphere in the summer hemisphere is the major source region of the measured low-energy electrons and ions. Those low-energy ion fluxes are enhanced abruptly, soon after the rapid chorus intensity modulation started, suggesting a relation between these two phenomena. Because the low-energy ions are fully covered in the ESA energy range, the density moment can be calculated much more accurately than the low-energy electrons. The density moment (<300 eV) in Figure 5f shows an enhancement after 10:50:50 UT together with density modulations. The density after 10:51 UT is about 7 times larger

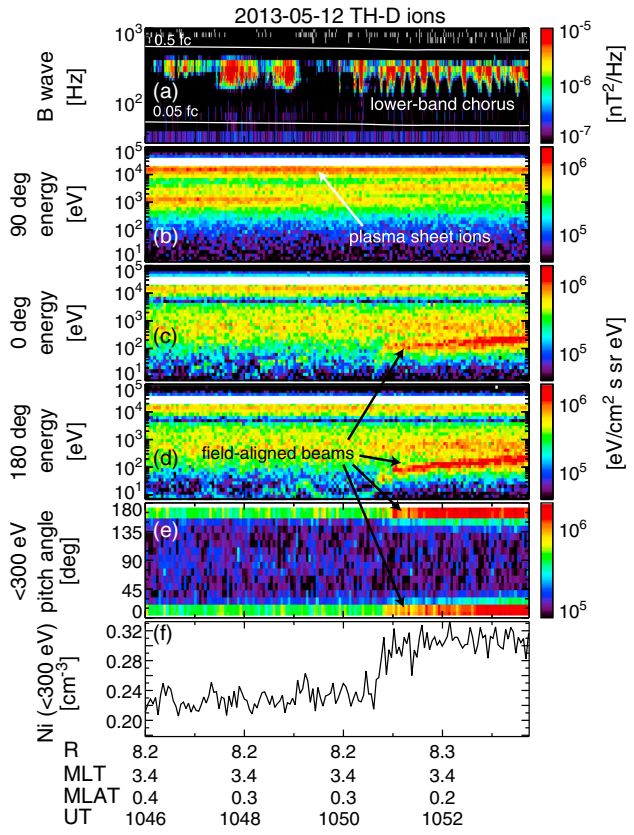

Figure 5. Same as Figure 2 but for 12 May 2013 observed by TH-D.

thanthe low-energy electron density shown in Figure 4f, and the ion energies are much higher than the spacecraft potential (~5.5 V), indicating that the low-energy plasma density can be calculated much more accurately by using the ion data.

The low-energy ion density is used to represent the cold plasma density for the *R* parameter calculation. Figure 6 shows that most of the chorus pulses (marked by red arrows) are associated with the ion density enhancements (blue arrows). The unmarked pulses are not correlated, but density enhancements are measured several seconds later for the 10:50:21 and 10:52:25 UT chorus pulses. As discussed in the previous event, this time lag is due perhaps to propagation time of low-energy plasma from the wave source region that could have a finite spread along the magnetic field lines. The *R* parameter also has small peaks due to the density enhancements (Figure 6c), although some pulses are obscured by fluctuations in the hot plasma population (Figure 6d). Nevertheless, the correlation between the chorus intensity and low-energy ion density suggests that enhancements in the low-energy plasma density likely modulate the chorus growth rate.

3.3. Events 3 and 4: 7 January 2010 and 2 January 2009

Figure 7 shows two more events observed during northern hemisphere winter to demonstrate that the properties described above can also be seen in other events. Both events in this figure show essentially the same feature as in the previous two events. Particularly, in the Figure 7 left event, the low-energy ion density enhancements (<800 eV) are seen mostly simultaneously with the chorus intensifications (Figures 7b and 7c). The field-aligned ion energy decreased between 06:01:10 and 06:03:30 UT (Figure 7g), and the larger ion density at lower energies during this period corresponds to larger amplitudes of chorus waves.

While the ion density below 2 keV modulates similarly to the chorus intensity in the Figure 7 right event, some of the ion density enhancements occur several seconds before or after the chorus intensifications. Such time lags are also seen in Figure 6 and could be because of finite travel times of low-energy ions from the wave-particle interaction region. Because source regions are spread over finite distances along magnetic field lines and may not be centered at the dipole equator, ion density enhancements would occur after wave intensifications if the satellites were located away from chorus generation regions. That limits the possibility of obtaining simultaneous correlation events to only when the satellites are located near the source region. In spite of this travel time issue, the correlations between the low-energy ion density and chorus intensity found in more than one event suggest that low-energy plasma contributes to chorus intensity modulation.

3.4. Superposed Epoch Analysis

We took all chorus wave enhancements shown in the four events above (61 events) and superposed them by taking epoch times as the peak amplitudes of individual chorus pulses. The solid line is the median of all events. Figure 8a shows a chorus intensity enhancement peaking at the zero epoch time by definition with

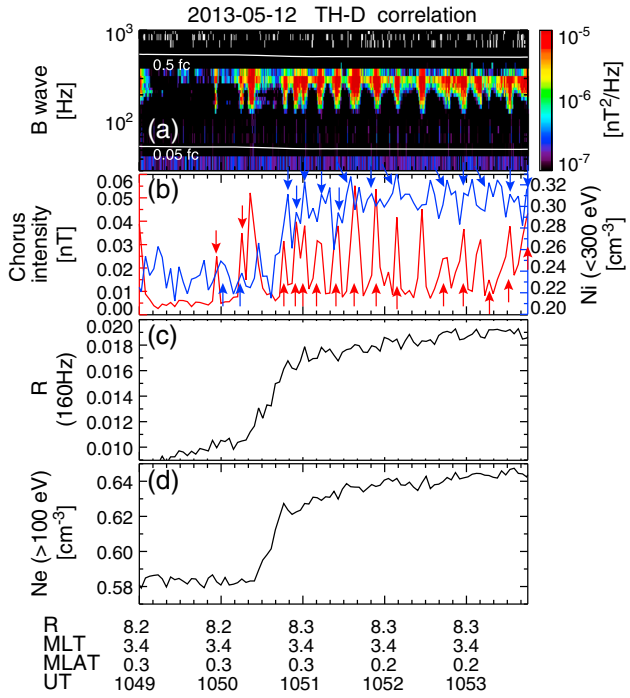

Figure 6. Same as Figure 3 but for 12 May 2013 by TH-D, except that the ion density moment and *R* parameter are given for <300 eV ions and 160 Hz.

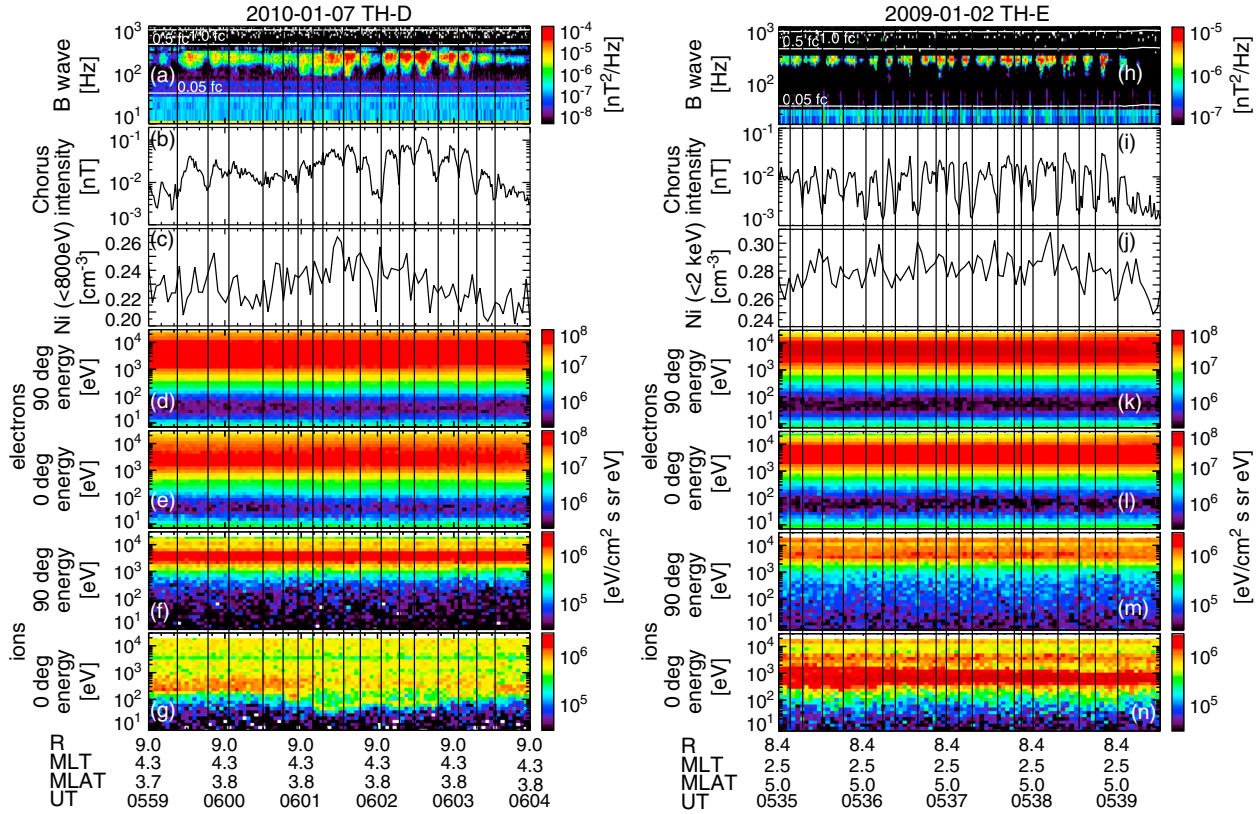

Figure 7. Two more events showing correlations between chorus intensity and low-energy ion density.

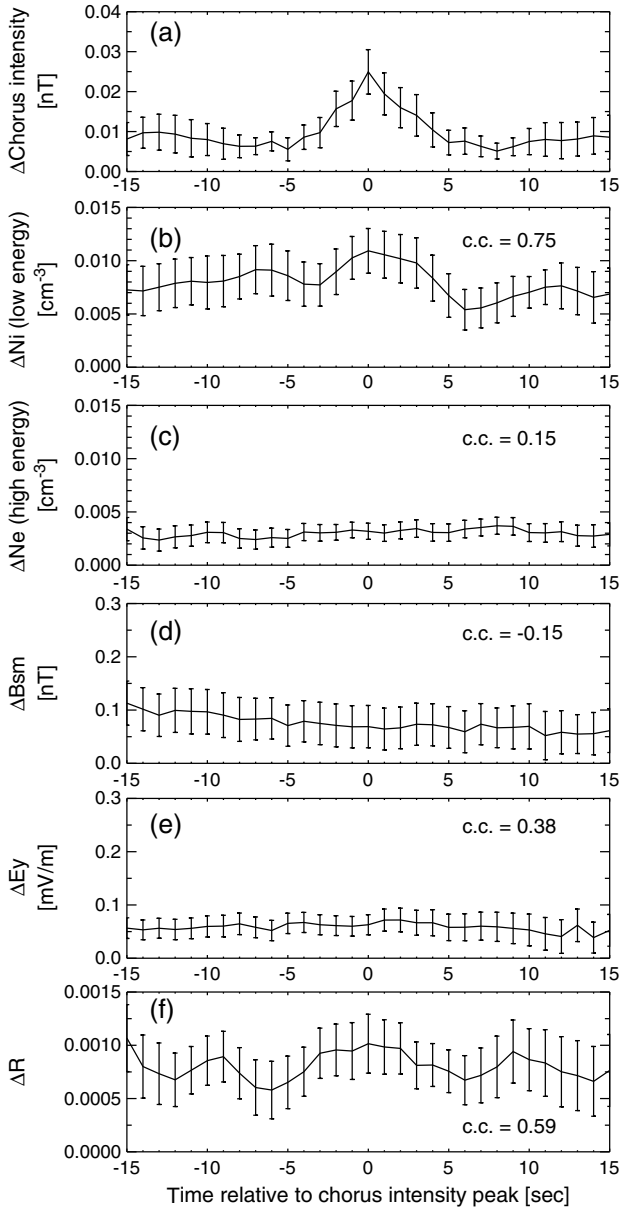

Figure 8. Superposed epoch analysis of (a) chorus intensity, (b) low-energy ion density, (c) high-energy electron density, (d) B_z, (e) E_y, and (f) R. The epoch times are those of maximum chorus intensity in individual chorus intensifications, and the baseline values are the minimum of each ±15 section in each event. The solid lines are median values, and the error bars indicate 95% confidence intervals using the *t*-distribution.

an ~±3 section of duration. The other parameters shown in Figure 8 are also superposed using the same chorus intensity peak times. In spite of large error bars, the low-energy ion density (Figure 8b) has a small peak around the chorus intensity peak time. The correlation coefficient between the median values of chorus intensity and low-energy ion density is 0.75 and corresponds to the density enhancement shown in earlier figures. This number becomes somewhat lower if the correlation is calculated event-by-event, perhaps due to uncertainties in ion flux measurements. However, a high correlation indicates that the modulation is real. This density variation results in positive wave growths as can be inferred from the corresponding enhancement in the R parameter (Figure 8f). It is particularly instructive to compare the correlation coefficient of the ions with the correlations of the other quantities in Figure 8, which are probably more representative of spurious correlations (i.e., noise). The large error bars arise from variable amplitudes of density and the measurement limitations described in section 3.1 may not allow for the detection of field-aligned density

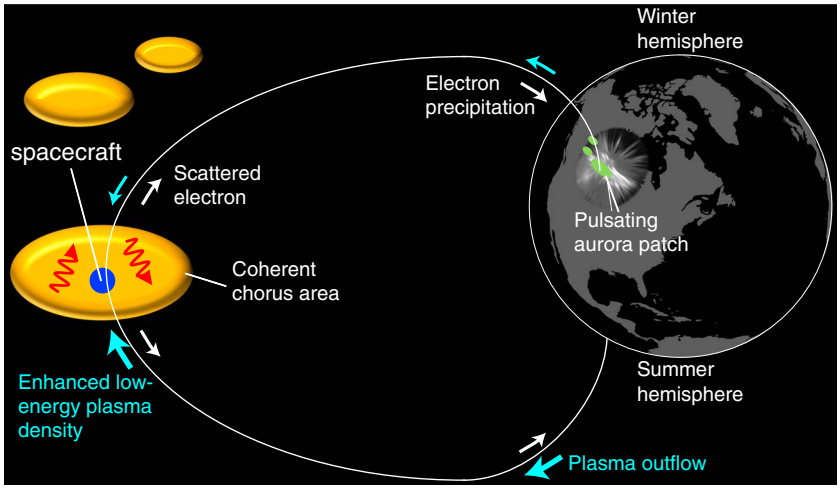

Figure 9. Schematic illustration of the chorus intensity modulation mechanism proposed in this study.

enhancements accurately. The low-energy ion density is the only parameter that shows a weak correlation with the chorus intensity. The high-energy electron density, ambient magnetic field, and electric field do not show any peak near the epoch time. This suggests that the low-energy ion density is likely the parameter that is related to the chorus intensification.

4. Discussion and Conclusion

By using burst mode particle and field observations recorded by THEMIS near the equator, we sought possible parameters that can potentially drive chorus intensity modulation in the postmidnight sector, which typically have a few tens of second periods. For the two events that we analyzed in detail, the satellites measured bidirectional chorus Poynting flux, indicating that the satellites are located near the chorus source region. The most notable feature we identified is the modulation of low-energy ion fluxes that are correlated with chorus intensity modulation. Those ions have ~100 eV energy and field-aligned pitch angles. The dominant fluxes are seen in 0° pitch angle in the northern hemisphere winter event (section 3.1) and in 180° in the northern hemisphere summer event (section 3.2). Those pitch angle preferences indicate that the low-energy ions originate in the sunlit ionosphere and modulate the equatorial density. Low-energy electrons ($<$~20 eV) are also seen to have field-aligned pitch angle distributions with the same pitch angle preference as the ions. However, the electron density is significantly underestimated due to the limited energy range and resolution of the electron instrument.

Assuming that those low-energy electrons and ions travel together to ensure the charge neutrality, the low-energy ion density moment can be used as a better representation of the cold plasma density, because the field-aligned ion beams are covered fully within the ESA energy range and their energies are sufficiently high to avoid effects from the spacecraft potential. The low-energy ion density moments are much larger than the low-energy electron density moment, indicating that the ion density gives a better estimate of the cold plasma density. We found that the *R* parameter is modulated similarly to the low-energy ion density. This indicates that the chorus growth rate is modulated by low-energy plasma density modulation. Since those low-energy electrons and ions do not resonate with lower band chorus waves, the electron density modulation is not due to direct wave-particle interaction but acts as variations in background media that modulate wave growth rates.

Ambient electric and magnetic fields are shown to be uncorrelated with the measured chorus intensity modulation. This supports the conclusion by *Oguti et al.* [1986], who found that the hydromagnetic wave model [*Coroniti and Kennel*, 1970] is not the mechanism that drives the chorus intensity modulation. Also, the lack of correlated modulation in the hot plasma density suggests that the chorus intensity modulation is not due to structures in plasma sheet electrons.

A suggested scenario is illustrated in Figure 9. Trapped energetic electrons interact with chorus waves and are scattered into the atmosphere. The precipitating energetic electrons increase the ionospheric density

and temperature and cause outflowing ions that travel along the magnetic field lines together with electrons for charge neutrality. The outflows occur in both hemispheres but are more intense from the summer hemisphere, where the ionospheric density is higher (southern hemisphere in this illustration). Based on the unidirectional pitch angle distribution, much of the outflowing plasma does not bounce back but sinks into the opposite hemisphere. Thus, the outflowing plasma does not accumulate near the equator, but the equatorial density modulates quasiperiodically; otherwise, density accumulations would eventually stop wave growths [*Gary et al*., 2012]. The low-energy plasma reaches the chorus generation region after a quarter bounce period and increases the equatorial plasma density. Density enhancements contribute to positive wave growths during the duration of the enhanced plasma density, leading to more scattering of energetic electrons into the atmosphere with the same duration of the enhanced waves. This positive feedback loop is suggested to act to drive repetitive modulation of chorus and pulsating aurora. While the equatorial density modulation is expected to stay intermittent throughout the lifetime of pulsating aurora, if the outflowing plasma is steady and fills the entire flux tube, chorus would not pulsate but drive nonpulsating diffuse aurora. The initiation of the feedback process is not measured in the present events, but we speculate that initial precipitation by substorm injection is a dynamically evolving process and drives varying outflows. This should be investigated in future studies using simultaneous measurements of injections and chorus.

Although plasma outflows in diffuse auroral regions are less explored compared to more intense outflows in discrete auroral regions, a recent study by *Liang et al*. [2015] showed using FAST satellite data that upgoing ions are co-located with diffuse auroral precipitation. Ionospheric density enhancements occur very rapidly in response to energetic electron precipitation [*Bösinger et al*., 1996; *Jones et al*., 2008; *Hosokawa et al*., 2010]. While much of the enhanced density is confined to 100–120 km altitude, modest density enhancements can be seen up to the highest-altitude limit (200 km) shown by *Jones et al*. [2008]. Those can potentially be the source of field-aligned beams measured by THEMIS.

Note that, because of the relatively long bounce periods of low-energy ions (several minutes for ~100 eV protons) [*Baumjohann and Treumann*, 1996], outflowing ions by a chorus burst do not affect the equatorial density immediately, and thus they do not affect the chorus element that caused the precipitation, but enhance chorus elements appearing sometime after it. This time lag implies that chorus intensity modulation builds up gradually after an electron injection. Although the Figure 6 event shows a sudden appearance of chorus and low-energy ions, those were not an initiation of chorus modulation but were likely present already before the satellite encounter, based on the lack of dipolarizations. Also, the ions do not necessarily come back to the position in the inertial frame, where the initial wave-particle interaction occurs, but drift with $E \times B$ speeds. Thus, the wave-particle interaction region will also move with $E \times B$ drift speeds. This suggestion is consistent with a known property of pulsating aurora, where pulsating auroral patches drift in $E \times B$ drift speeds rather than in magnetic drift speeds of plasma sheet electrons [*Nakamura and Oguti*, 1987]. Although a flux tube with high cold plasma density has been considered in the models by *Davidson and Chiu* [1987] and *Demekhov and Trakhtengerts* [1994], our results differ from their models in a sense that the cold plasma density modulation determines chorus intensity modulation.

Since we found a positive correlation between density and wave intensity modulations, these events can be classified as density enhancement events in the *Li et al*. [2011] categorization. A difference is that only part of the electron distribution is seen near the low-energy limit of the ESA instrument, while density enhancements in the Li et al. events were measured in tens of eV up to a few hundred eV electrons. While the events presented here would be classified as density depletion events in Li et al., the lack of density depletions in the particle data is probably because the spacecraft potential density is affected by photoelectrons [*Malaspina et al*., 2014].

Finally, we should note a few limitations of the present study. This study only shows four events as case studies. Although these events suggest that the correlation between chorus intensity and low-energy ion density is not coincidental, it is still an open question of how commonly modulation of low-energy plasma density occurs in correlation with chorus intensity modulation. The correlation between plasma density and chorus intensity is not perfect, and the finite time lags seen for some spikes may be attributed to finite distances from wave source regions that may not always be close to the satellite locations, although we chose events where the satellites were close to the source region based on the Poynting flux directions. In addition, the R parameter changes are relatively small, suggesting that the growth rate changes are also small. We expect that

even small changes could give substantial wave growth if plasma sheet electrons are marginally stable before density enhancements. Chorus generation process involves nonlinear growth processes and propagation effects, so that a small difference in linear wave growth rates may give rise to significantly different chorus wave amplitudes through nonlinear wave processes occurring on preexisting weak waves generated through the linear process [*Omura and Nunn*, 2011; *Tao*, 2014]. Convective growths along wave raypaths should be calculated to examine if the *R* parameter changes can give significant wave amplifications. It requires profiles of enhanced densities along magnetic field lines, which are difficult to obtain from single satellite observations. While field-aligned beams have been considered in wave growth calculations and shown to increase wave growth rates [e.g., *Tokar and Gurnett*, 1985; *Leubner*, 2000], they used energetic beams that resonate with whistler mode waves through cyclotron interaction. A modeling with lower-energy beams should be conducted for evaluating wave amplification by enhanced low-energy plasma density.

Acknowledgments

This work was supported by NASA grants NNX12AJ57G, NNX13AI61G, NNX11AR64G, NNX14AI18G, NNX15AF61G, and NAS5-02099 and NSF grants AGS-1101903, AGS-1242356, AGS-1405054, and PLR-1341359. The French involvement (SCM instruments) on THEMIS is supported by CNES and CNRS-INSU. The THEMIS data used in this study are publically available through http://themis.ssl.berkeley.edu/.

Michael Liemohn thanks Yue Chen and two other reviewers for their assistance in evaluating this paper.

References

Angelopoulos, V. (2008), The THEMIS mission, *Space Sci. Rev.*, *141*, 5–34, doi:10.1007/s11214-008-9336-1.

Auster, H., et al. (2008), The THEMIS fluxgate magnetometer, *Space Sci. Rev.*, *141*, 235–264.

Baumjohann, W., and R. A. Treumann (1996), *Basic Space Plasma Physics*, Imperial College Press, London.

Bonnell, J. W., et al. (2008), The Electric Field Instrument (EFI) for THEMIS, *Space Sci. Rev.*, *141*(1–4), 303–341.

Bösinger, T., K. Kaila, R. Rasinkangas, P. Pollari, J. Kangas, V. Trakhtengerts, and A. Demekhov (1996), An EISCAT study of a pulsating auroral arc: Simultaneous ionospheric electron density, auroral luminosity and magnetic field pulsations, *J. Atmos. Terr. Phys.*, *58*, 23–35.

Chappell, C. R., M. M. Huddleston, T. E. Moore, B. L. Giles, and D. C. Delcourt (2008), Observations of the warm plasma cloak and an explanation of its formation in the magnetosphere, *J. Geophys. Res.*, *113*, A09206, doi:10.1029/2007JA012945.

Contel, L., et al. (2008), First results of the THEMIS search coil magnetometers, *Space Sci. Rev.*, *141*(1–4), 509–534.

Coroniti, F. V., and C. F. Kennel (1970), Electron precipitation pulsations, *J. Geophys. Res.*, *75*(7), 1279–1289, doi:10.1029/JA075i007p01279.

Cully, C. M., R. E. Ergun, K. Stevens, A. Nammari, and J. Westfall (2008), The THEMIS digital fields board, *Space Sci. Rev.*, *141*, 343–355.

Cuperman, S., and R. W. Landau (1974), On the enhancement of the whistler mode instability in the magnetosphere by cold plasma injection, *J. Geophys. Res.*, *79*(1), 128–134, doi:10.1029/JA079i001p00128.

Davidson, G. T., and Y. T. Chiu (1987), A nonlinear model of wave-particle interactions in the trapped radiation belts: Auroral pulsation solutions, *Geophys. Res. Lett.*, *14*(11), 1166–1169, doi:10.1029/GL014i011p01166.

Demekhov, A. G., and V. Y. Trakhtengerts (1994), A mechanism of formation of pulsating aurorae, *J. Geophys. Res.*, *99*(A4), 5831–5841, doi:10.1029/93JA01804.

Gary, S. P., K. Liu, R. E. Denton, and S. Wu (2012), Whistler anisotropy instability with a cold electron component: Linear theory, *J. Geophys. Res.*, *117*, A07203, doi:10.1029/2012JA017631.

Horwitz, J. L., C. R. Baugher, C. R. Chappell, E. G. Shelley, and D. T. Young (1982), Conical pitch angle distributions of very low-energy ion fluxes observed by ISEE 1, *J. Geophys. Res.*, *87*(A4), 2311–2320, doi:10.1029/JA087iA04p02311.

Hosokawa, K., Y. Ogawa, A. Kadokura, H. Miyaoka, and N. Sato (2010), Modulation of ionospheric conductance and electric field associated with pulsating aurora, *J. Geophys. Res.*, *115*, A03201, doi:10.1029/2009JA014683.

Johnstone, A. D. (1983), The mechanism of pulsating aurora, *Ann. Geophys.*, *1*, 397–410.

Jones, S. L., et al. (2008), PFISR and ROPA observations of pulsating aurora, *J. Atmos. Sol. Terr. Phys.*, *71*, 708, doi:10.1016/j.jastp.2008.10.004.

Kennel, C. F., and H. E. Petschek (1966), Limit on stably trapped particle fluxes, *J. Geophys. Res.*, *71*(1), 1–28, doi:10.1029/JZ071i001p00001.

Leubner, M. P. (2000), Theoretical interpretation of Jupiter's multibanded whistler mode emission, *J. Geophys. Res.*, *105*(A9), 21,261–21,265, doi:10.1029/1999JA000393.

Li, W., J. Bortnik, R. M. Thorne, Y. Nishimura, V. Angelopoulos, and L. Chen (2011), Modulation of whistler mode chorus waves: 2. Role of density variations, *J. Geophys. Res.*, *116*, A06206, doi:10.1029/2010JA016313.

Li, W., J. Bortnik, Y. Nishimura, R. M. Thorne, and V. Angelopoulos (2013a), The origin of pulsating aurora: Modulated whistler mode chorus waves, in *Auroral Phenomenology and Magnetospheric Processes: Earth And Other Planets*, edited by A. Keiling et al., AGU, Washington, D. C.

Li, W., J. Bortnik, R. M. Thorne, C. M. Cully, L. Chen, V. Angelopoulos, Y. Nishimura, J. B. Tao, J. W. Bonnell, and O. LeContel (2013b), Characteristics of the Poynting flux and wave normal vectors of whistler-mode waves observed on THEMIS, *J. Geophys. Res. Space Physics*, *118*, 1461–1471, doi:10.1002/jgra.50176.

Liang, J., E. Donovan, Y. Nishimura, B. Yang, E. Spanswick, K. Asamura, T. Sakanoi, D. Evans, and R. Redmon (2015), Low-energy ion precipitation structures associated with pulsating auroral patches, *J. Geophys. Res. Space Physics*, doi:10.1002/2015JA021094, in press.

Malaspina, D. M., R. E. Ergun, A. Sturner, J. R. Wygant, J. W. Bonnell, A. Breneman, and K. Kersten (2014), Chorus waves and spacecraft potential fluctuations: Evidence for wave-enhanced photoelectron escape, *Geophys. Res. Lett.*, *41*, 236–243, doi:10.1002/2013GL058769.

McFadden, J. P., C. W. Carlson, D. Larson, J. Bonnell, F. Mozer, V. Angelopoulos, K.-H. Glassmeier, and U. Auster (2008), THEMIS ESA first science results and performance issues, *Space Sci. Rev.*, *141*(1–4), 477–508.

Nakamura, R., and T. Oguti (1987), Drifts of auroral structures and magnetospheric electric fields, *J. Geophys. Res.*, *92*(A10), 11,241–11,247, doi:10.1029/JA092iA10p11241.

Ni, B., R. M. Thorne, N. P. Meredith, R. B. Horne, and Y. Shprits (2011), Resonant scattering of plasma sheet electrons leading to diffuse auroral precipitation: 2. Evaluation for whistler-mode chorus waves, *J. Geophys. Res.*, *116*, A04219, doi:10.1029/2010JA016233.

Nishimura, Y., et al. (2010), Identifying the driver of pulsating aurora, *Science*, *330*, 81–84.

Nishimura, Y., et al. (2011), Multievent study of the correlation between pulsating aurora and whistler mode chorus emissions, *J. Geophys. Res.*, *116*, A11221, doi:10.1029/2011JA016876.

Oguti, T., K. Hayashi, T. Yamamoto, J. Ishida, T. Higuchi, and N. Nishitani (1986), Absence of hydromagnetic waves in the magnetospheric equatorial region conjugate with pulsating auroras, *J. Geophys. Res.*, *91*(A12), 13,711–13,715, doi:10.1029/JA091iA12p13711.

Omura, Y., and D. Nunn (2011), Triggering process of whistler mode chorus emissions in the magnetosphere, *J. Geophys. Res.*, *116*, A05205, doi:10.1029/2010JA016280.

Omura, Y., Y. Katoh, and D. Summers (2008), Theory and simulation of the generation of whistler-mode chorus, *J. Geophys. Res.*, *113*, A04223, doi:10.1029/2007JA012622.

Santolík, O., D. A. Gurnett, J. S. Pickett, M. Parrot, and N. Cornilleau-Wehrlin (2004), A microscopic and nanoscopic view of storm-time chorus on 31 March 2001, *Geophys. Res. Lett.*, *31*, L02801, doi:10.1029/2003GL018757.

Tagirov, V. . R., V. . S. Ismagilov, E. . E. Titova, V. . A. Arinin, A. . M. Perlikov, J. Manninen, T. Turunen, and K. Kaila (1999), Auroral pulsations and accompanying VLF emissions, *Ann. Geophys.*, *17*, 66–78, doi:10.1007/s00585-999-0066-9.

Tao, X. (2014), A numerical study of chorus generation and the related variation of wave intensity using the DAWN code, *J. Geophys. Res. Space Physics*, *119*, 3362–3372, doi:10.1002/2014JA019820.

Thorne, R. M., B. Ni, X. Tao, R. B. Horne, and N. P. Meredith (2010), Scattering by chorus waves as the dominant cause of diffuse auroral precipitation, *Nature*, *467*, 943–946, doi:10.1038/nature09467.

Tokar, R. L., and D. A. Gurnett (1985), The propagation and growth of whistler mode waves generated by electron beams in Earth's bow shock, *J. Geophys. Res.*, *90*(A1), 105–114, doi:10.1029/JA090iA01p00105.

Tsuruda, K., S. Machida, T. Oguti, S. Kokubun, K. Hayashi, T. Kitamura, O. Saka, and T. Watanabe (1981), Correlations between the very low frequency chorus and pulsating aurora observed by low-light-level television at L-4.4, *Can. J. Phys.*, *59*, 1042–1048, doi:10.1139/p81-137.

Tsurutani, B. T., G. S. Lakhina, and O. P. Verkhoglyadova (2013), Energetic electron (>10 keV) microburst precipitation, 5–15 s X-ray pulsations, chorus, and wave-particle interactions: A review, *J. Geophys. Res. Space Physics*, *118*, 2296–2312, doi:10.1002/jgra.50264.

Wu, S., R. E. Denton, and W. Li (2013), Effects of cold electron density on the whistler anisotropy instability, *J. Geophys. Res. Space Physics*, *118*, 765–773, doi:10.1029/2012JA018402.